JOURNAL OF PROPULSION AND POWER
Vol. 11, No. 5, September–October 1995

Thermohydrodynamic Analysis of Fluid Film Bearings for Cryogenic Applications

Luis San Andres*
Texas A&M University, College Station, Texas 77843

A thermohydrodynamic analysis and computer program for prediction of the static and dynamic force response of hydrostatic journal bearings, annular seals, or damping bearings, and fixed arc-pad bearings are presented. The study includes the most important flow characteristics found in cryogenic fluid film bearings such as flow turbulence, fluid inertia, liquid compressibility, and thermal effects. Numerical results detail a comparison of the static performance and dynamic force coefficients for a six-recess hydrostatic bearing and a damping bearing-seal for the Space Shuttle Main Engine high-pressure oxidizer turbopump. The calculations indicate that turbulent-flow, externally pressurized bearings support the expected loads with moderate journal center eccentricities and with force coefficients of relevant magnitude for this critical application.

Nomenclature

A_o = $C_d\pi d_o^2/4$, equivalent orifice area, m²
A_r = bl, recess area, m²
b = recess circumferential length, m
C_d = empirical orifice discharge coefficient
C_{ij} = damping force coefficients, Ns/m
C_p = specific heat, J/kg·K
c, c_* = radial clearance, characteristic clearance ($=\{c(y)\}_{\min}$), m
D = journal diameter, m
d_o = orifice diameter, m
e_X, e_Y = journal center displacements, m
F_X, F_Y = fluid film forces along $\{X, Y\}$ axes, N
f_J, f_B = $a_m[1 + (c_m r_{J,B}/H + b_m/R_{J,B})^{e_m}]$, turbulent friction factors based on Moody's equation, $a_m = 0.001375$; $b_m = 5 \times 10^5$; $c_m = 10^4$; $e_m = 1/3.0$
H, H_r = film thickness, recess depth, m
K_{ij} = stiffness force coefficients, N/m
k_J, k_B = $f_J R_J$, $f_B R_B$, turbulent shear parameters
k_r = $Re_r^{0.681}/7.753$, turbulent shear flow recess parameter
k_x, k_y = $(k_J + k_B)/2$
L = bearing or seal axial length, m
l = recess axial lengths, m
M_{ij} = inertia force coefficients, kg
M_r = $\alpha R\Omega\sqrt{\beta_\rho \rho_r}$, recess flow Mach number due to journal rotation
$\dot{m}$ = flow rate over differential segments, kg/s
$N_{\rm rec}$ = number of bearing recesses
$\boldsymbol{n}$ = normal vector to recess boundary
P = fluid pressure, N/m²
P_s, P_a, P_r = external supply, ambient, and recess pressures, N/m²
P_X, P_Y = perturbed (dynamic pressures), N/m³
Q_r = mass flow rate from recess to land, kg/s
Q_s = heat flux to bearing and journal surfaces, W/m²
R = journal radius, m
R_B = $\rho H\sqrt{U^2 + V^2}/\mu$, Reynolds number relative to bearing surface
Re_c = $\rho_* R\Omega c_*/\mu_*$, nominal circumferential flow Reynolds number
Re_H = $\rho_e R\Omega H_e/\mu_e$, Reynolds number at recess edges
Re_r = $\rho_r R\Omega(H_r + H)/\mu_r$, Reynolds number at recess volume due to rotation
R_J = $\rho H\sqrt{(U - \Omega R)^2 + V^2}/\mu$, Reynolds number relative to journal surface
r_J, r_B = mean roughness depth at journal and bearing surfaces, m
T = bulk-flow fluid temperature, K
T_{or}^r = $\tau_{xz}^H A_r R$, torque over a recess, N-m
T_s = inlet supply temperature, K
t = time, s
U, V = bulk-flow velocities in circumferential and axial directions, m/s
$\boldsymbol{U}$ = $U\boldsymbol{i} + V\boldsymbol{j}$
X, Y = inertial coordinate system
x, y, z = $(0, \pi D)$, $(0, L)$, $[0, H(x, y, t)]$, coordinates defining thin film flow region
α = $(U|_{y=0})/(\Omega R)$, circumferential velocity entrance swirl factor
β_ρ = $(1/\rho)(\partial\rho/\partial P)_T$, liquid compressibility factor, m²/N
β_T = $-(1/\rho)(\partial\rho/\partial T)_p$, volumetric expansion coefficient, 1/K
$\zeta_{x,y}$ = $1.95/Re_H^{0.43}$, 0, recess edge loss coefficients
η = $H/(H_r + H)$, ratio of land film thickness to recess depth
μ = fluid viscosity, Ns/m²
$\xi_{su,d}$ = entrance loss coefficients at up-, downstream recess edges
$\xi_{x,y}$ = empirical entrance loss coefficients in x, y directions
ρ = fluid density, kg/m³
τ_{xz}, τ_{yz} = wall shear stresses
Ω = rotational speed of journal, rad/s
ω = excitation or whirling frequency, rad/s
$\forall_r$ = $(H_r + H)A_r + \forall_s$, recess volume of hydrostatic bearing, m³
$\forall_s$ = volume of orifice supply line, m³

Subscripts

a = ambient or discharge conditions
B = bearing
e = entrance or recess edge conditions
i, j = first-order perturbations ($i, j \rightarrow X, Y$ directions)
J = journal

Received July 5, 1994; revision received Sept. 15, 1994; accepted for publication Sept. 30, 1994.
*Associate Professor, Mechanical Engineering Department.

r = recess conditions
s = supply conditions
$*$ = characteristic values

I. Introduction

HYDROSTATIC Journal Bearings (HJBs) are the ideal candidates to replace rolling element bearings as support elements in cryogenic turbomachinery. These bearings along with hydrostatic annular seals will be used for primary space-power applications due to their long lifetime, low friction and wear, significant load capacity, and large direct stiffness and damping force coefficients. Fluid film bearings, unlike rolling element bearings, have no diameter × rotational speed (DN) limit. Rotating machinery, free of this constraint, can operate at higher speeds with better efficiency and reduced overall weight and size. Durability in fluid film bearings is assured by the absence of contact between stationary and moving parts during steady-state operation, while long life reduces the frequency of required overhauls. Despite these attractive features, dynamic stability considerations and thermal phenomena along with two-phase flow operation are primary concerns for high-speed operation in bearings with large pressure differentials. Fluid film bearing stability is essentially related to hydrodynamic and liquid compressibility effects, whereas thermal effects are of importance due to flow turbulence with substantial energy dissipation.

San Andres[1-3] provides a comprehensive literature review on the subject of hydrostatic bearings and annular seals relevant to cryogenic liquid applications. Kurtin et al.[4] and Childs and Hale[5] describe a test facility for the measurement of loads and frequency domain identification of dynamic force coefficients in turbulent-flow, water-lubricated hydrostatic bearings, and annular pressure seals. Tests are routinely performed for bearings of different geometries and at journal speeds ranging from 10,000 to 25,000 rpm and pressure supplies from 4 to 7 MPa. Lindsey[6] has recently reported measured force coefficients for short-length annular seals with uniform, convergent, and divergent axial clearances. Kurtin et al.,[4] Mosher,[7] and Franchek et al.[8,9] report experimental data for the static load and dynamic force coefficients of water-lubricated hydrostatic bearings at the operating conditions noted. The test results refer to bearing clearances from 76 to 125 μm, different recess pressure ratios and shapes, smooth and rough bearing surfaces, and radial vs angled liquid orifice injection.

Along with the experimental investigations, San Andres[2] developed a turbulent-inertial bulk flow analysis for prediction of the performance characteristics of orifice-compensated HJBs with variable-property fluids, and demonstrated the advantages of the model when compared to traditional approaches based on laminar-flow, classical lubrication theory. Yang et al.[10,11] then introduced a thermohydrodynamic (THD) analysis for the prediction of the static and dynamic performance characteristics of cryogenic liquid annular seals and hydrostatic journal bearings. Shear parameters based on friction factors derived from Moody's formulas account for flow turbulence. The effects of fluid compressibility and temperature variation in the bearing recesses are included. Comparisons of experimental results vs numerical predictions for water-lubricated hydrostatic bearings with radial fluid injection are reported.[4,7,9] The correlations validate the numerical models,[2,11] although accurate theoretical results depend greatly on the knowledge of the bearing operating clearance, bearing surface conditions, and most importantly, on the orifice discharge coefficients. Numerical results show the effects of fluid compressibility to be significant for liquid hydrogen (LH_2) hydrostatic bearings with the potential of a stability indicator worse than that found in plain journal bearings due to pneumatic hammer at the bearing recesses.[2] Predictions from the THD model[11] correlate well with measured temperatures for the preburner impeller rear wear-ring seal of the Space Shuttle Main Engine (SSME) high-pressure oxidizer turbopump (HPOTP). Calculations performed for a high-speed, rough-surface liquid oxygen (LO_2) seal also predict a large temperature rise and the onset of two-phase flow conditions (liquid boiling) at moderate shaft eccentricities despite the large pressure differential across the seal. It is imperative to note that large temperature rises in cryogenic liquid seals and bearings can lead to thermal solid distortions affecting the operating clearance and may cause a significant reduction on the direct (hydrostatic) stiffnesses.

This article presents the thermohydrodynamic analysis of variable-property, fluid film bearings for cryogenic applications. The bearings studied include hydrostatic pad bearings with rectangular recesses, annular pressure seals or damping bearings, and cylindrical rigid-pad hydrodynamic bearings. The theoretical model refers to bearings of asymmetric geometry, nonuniform pressure discharges, and arbitrary clearance distribution. The motion of a liquid on the thin-film annular region of a fluid film bearing is described by a set of mass, momentum conservation, and energy transport equations for the primitive turbulent bulk-flow variables, and accompanied by realistic thermophysical state equations for evaluation of the fluid material properties. Zeroth-order equations describe the fluid flowfield for a journal static equilibrium position, while first-order linear equations govern the fluid flow for small-amplitude journal center translational motions and journal axis conical motions.

The solution to the zeroth-order flowfield equations provides the bearing flow rate, load capacity, torque, and restoring moments due to journal misalignment. The solution to the first-order equations determines the rotordynamic force and moment coefficients due to journal lateral and angular motions. For lateral shaft (journal) excursions, the dynamic force characteristics refer to the stiffness K_{ij}, damping C_{ij}, and added mass M_{ij} coefficients, and related to the dynamic forces by

$$\begin{bmatrix} F_X \\ F_Y \end{bmatrix} = \begin{bmatrix} F_{X0} \\ F_{Y0} \end{bmatrix} - \begin{bmatrix} K_{XX} & K_{XY} \\ K_{YX} & K_{YY} \end{bmatrix} \begin{bmatrix} \Delta X \\ \Delta Y \end{bmatrix} - \begin{bmatrix} C_{XX} & C_{XY} \\ C_{YX} & C_{YY} \end{bmatrix} \begin{bmatrix} \Delta \dot{X} \\ \Delta \dot{Y} \end{bmatrix} - \begin{bmatrix} M_{XX} & M_{XY} \\ M_{YX} & M_{YY} \end{bmatrix} \begin{bmatrix} \Delta \ddot{X} \\ \Delta \ddot{Y} \end{bmatrix} \quad (1)$$

where $\Delta X(t)$ and $\Delta Y(t)$ are the components of the journal-center dynamic displacement about an equilibrium position. The dynamic-force coefficients defined by Eq. (1) are important measures of bearing dynamic performance since they influence the system critical speeds, the resonant amplitude response, and the stability of the rotor-bearing system.

II. Mathematical Model

A. Governing Equations for Turbulent Fluid Film Flows

Figures 1 and 2 show the schematic drawings of a hydrostatic bearing and a damping bearing (annular seal) considered for the analysis. Large pressure gradients typical of cryogenic bearings cause high-axial turbulent-flow Reynolds numbers, and the effect of turbulent mixing far outweighs molecular diffusivity. The temperature rise produced by viscous dissipation tends to be distributed uniformly across the film thickness, and thus, temperature gradients in the cross-film coordinate are confined to turbulent-flow boundary layers adjacent to the bounding (bearing and journal) surfaces.[12] Furthermore, in the absence of regions of reversed flow or recirculation, the fluid velocity field presents the same characteristics as discussed above. The flow studied is confined to the thin annular region between an inner rotating journal and a stationary bearing. The considerations detailed allow the

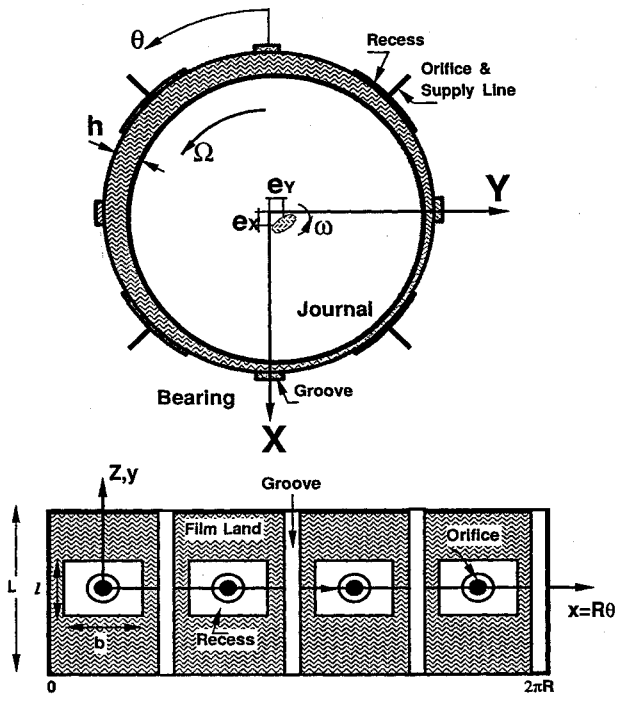

Fig. 1 Geometry of hydrostatic pad bearing.

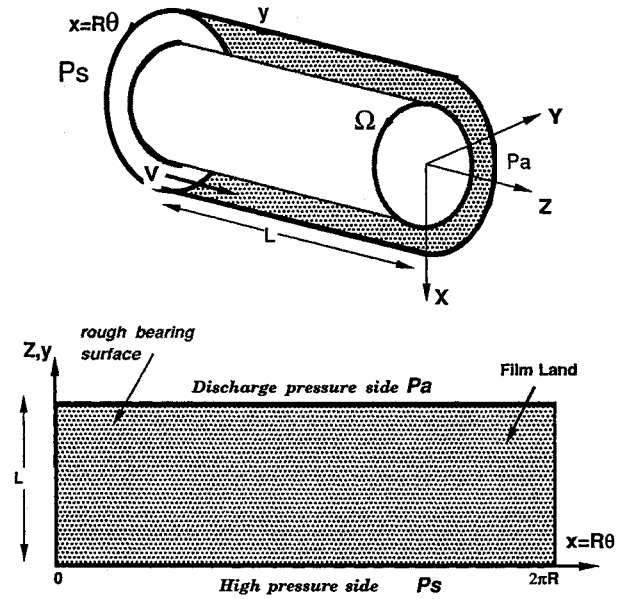

Fig. 2 Geometry of annular (damper) seal.

fluid motion to be described by a set of bulk-flow governing equations[10,11]:

Continuity equation

$$\frac{\partial(\rho H)}{\partial t} + \frac{\partial(\rho HU)}{\partial x} + \frac{\partial(\rho HV)}{\partial y} = 0 \tag{2}$$

Circumferential-momentum equation

$$\frac{\partial(\rho HU)}{\partial t} + \frac{\partial(\rho HU^2)}{\partial x} + \frac{\partial(\rho HUV)}{\partial y} = -H\frac{\partial P}{\partial x} + \tau_{xz}|_0^H \tag{3}$$

Axial-momentum equation

$$\frac{\partial(\rho HV)}{\partial t} + \frac{\partial(\rho HUV)}{\partial x} + \frac{\partial(\rho HV^2)}{\partial y} = -H\frac{\partial P}{\partial y} + \tau_{yz}|_0^H \tag{4}$$

Energy-transport equation

$$C_p\left[\frac{\partial(\rho HT)}{\partial t} + \frac{\partial(\rho HUT)}{\partial x} + \frac{\partial(\rho HVT)}{\partial y}\right] + Q_s = T\beta_T H\left(\frac{\partial P}{\partial t} + U\frac{\partial P}{\partial x} + V\frac{\partial P}{\partial y}\right) + R\Omega\tau_{xz}|^H - U\tau_{xz}|_0^H - V\tau_{yz}|_0^H \tag{5}$$

where the bulk-flow primitive variables (U, V, P, and T) are defined as average quantities across the film thickness, and Q_s represents the heat flux from the fluid film towards the journal and bearing surfaces.

The wall shear stresses are calculated according to the bulk-flow theory for turbulence in thin film flows[13,14]:

$$\tau_{xz}|_0^H = -\frac{\mu}{H}\left(k_x U - k_J\frac{R\Omega}{2}\right)$$

$$\tau_{yz}|_0^H = -\frac{\mu}{H}(k_y V) \tag{6}$$

$$\tau_{xz}|^H = \frac{H}{2}\frac{\partial P}{\partial x} + \frac{\mu}{4H}[Uk_B - (U - R\Omega)k_J]$$

where the turbulent shear parameters (k_x, k_y) and (k_J, k_B) are local functions of the Reynolds numbers and friction factors based on Moody's formulas.[15]

B. Mass Conservation at a Bearing Recess

The analysis of turbulent flow in a HJB recess is complicated and not yet fully studied on its three-dimensional complexity.[16–18] Fundamental measurements have shown non-uniform pressures within a bearing recess of shallow depth, and with a hydrodynamic pressure rise generated on its downstream section.[19,20] Nonetheless, approximate formulations capturing the physics of the flow in its global sense are still of value to predict the overall flow rate and force performance of bearings with pressurized recesses.[20] The continuity equation at a recess of a hydrostatic bearing relates the global balance among the flow through the orifice restrictor, the recess outflow into the film lands Q_r, and the temporal change of fluid mass within the recess volume $\forall_r$, and expressed as

$$A_0\sqrt{2\rho_r(P_s - P_r)} = Q_r + \rho_r\frac{\partial \forall_r}{\partial t} + \rho_r \forall_r\left(\beta_p\frac{\partial P}{\partial t} - \beta_T\frac{\partial T}{\partial t}\right)_r \tag{7}$$

where

$$Q_r = \int_{\Gamma_r} \rho H(\boldsymbol{U}\cdot\boldsymbol{n})\, d\Gamma \tag{8}$$

is the mass flow rate across the recess edges Γ_r and entering the film lands; and (β_p, β_T) are the fluid compressibility and volumetric expansion coefficients, respectively. In general,

$$\beta_p,\ \beta_T \begin{cases} = 0 & \text{for incompressible liquids} \\ = 1/P,\ 1/T & \text{for ideal gases} \\ > 0 & \text{for cryogenic liquids} \end{cases} \tag{9}$$

For purely hydrostatic operation, a uniform recess pressure is desirable to increase the bearing load capacity. This condition can be achieved by deepening the bearing recesses, although a minimum recess volume is required to avoid the characteristic pneumatic hammer instability associated with fluid compressibility.[21] For hybrid operation (combined hydrostatic–hydrodynamic), a pressure rise occurs due to the journal rotation,[20] as shown in Fig. 3. A simple one-dimen-

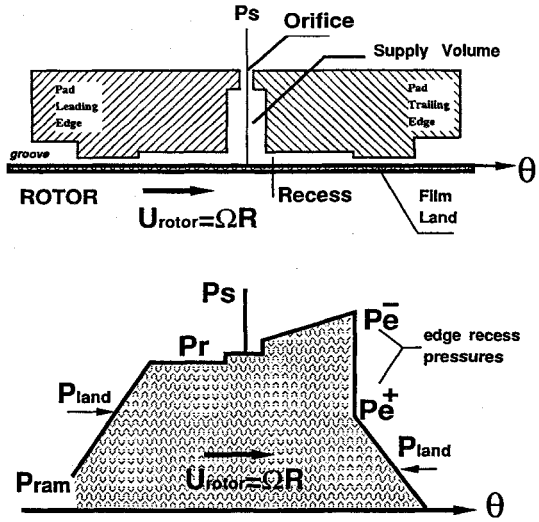

Fig. 3 Conceptual description of pressure rise and drop at recess edge of a hydrostatic bearing, and pressure ram effect at leading edge of bearing pad.

sional step-bearing model predicts the pressure rise just in front of the downstream recess edge P_e^- as[22]

$$P_e^- = \left\{ P_r - \frac{b\eta^2 \mu k_r}{2H^2(1 - M_r^2)} \cdot \left[U\eta \left(\frac{\rho_e}{\rho_r} \right) - \frac{V_r}{2} \right] \cdot \boldsymbol{n} \right.$$

$$\text{for} \quad (\boldsymbol{U} \cdot \boldsymbol{n}) > 0, \quad \begin{matrix} \text{in } x \text{ direction} \\ \text{in } y \text{ direction} \end{matrix} \tag{10}$$

where $\boldsymbol{n}$ is the normal to the recess boundary Γ_r, and

$$\boldsymbol{U} = U\boldsymbol{i} + V\boldsymbol{j}, \qquad \boldsymbol{V}_r = R\Omega\boldsymbol{i} + 0\boldsymbol{j} \tag{11}$$

Refer to the Nomenclature for a description of all variables. The local acceleration of fluid from the deep recess to the film lands causes a sudden pressure drop at the recess edges (see Fig. 3). The pressure at the entrance to the film lands is modeled by simple Bernoulli-type relations based on the turbulent flow theory developed by Constantinescu and Galetuse[22] and Artiles et al.[23]:

$$P_e^+ = P_e^- - (\rho_e/2)(1 + \zeta_i)(1 + \xi_i)[1 - \eta^2(\rho_e/\rho_r)](\boldsymbol{U} \cdot \boldsymbol{n})^2$$

$$(\boldsymbol{U} \cdot \boldsymbol{n}) > 0 \tag{12}$$

where $\zeta_i = \{\zeta_x, \zeta_y\}$, $\xi_i = \{\xi_x, \xi_y\}$ are empirical entrance loss coefficients. The pressure at the entrance of an annular pressure seal can be obtained similarly by using a Bernoulli-type relation. The corresponding expression is given later in the boundary conditions section.

C. Global Energy Balance Equation at a Recess

A global energy balance equation at a hydrostatic bearing recess shows the heat carry-over (advection) and mixing effects, and the friction heat generation (dissipation) in the recess (see Fig. 4):

$$C_p \frac{\partial(\rho T)}{\partial t} \forall_r + C_p \left(\sum \dot{m}_d T_d + 2 \sum \dot{m}_{\text{side}} T_{\text{side}} \right)$$

$$= C_p \left(\sum \dot{m}_u T_u + Q_r T_s \right) + T_{or}^r \Omega \tag{13}$$

where T_{or}^r is the shear-induced torque over the recess area, Q_r is the total mass flow rate through the supply orifice, $\forall_r$ is the recess volume, and the subscripts u, d, and side refer to the upstream, downstream, and side edges of a rectangular

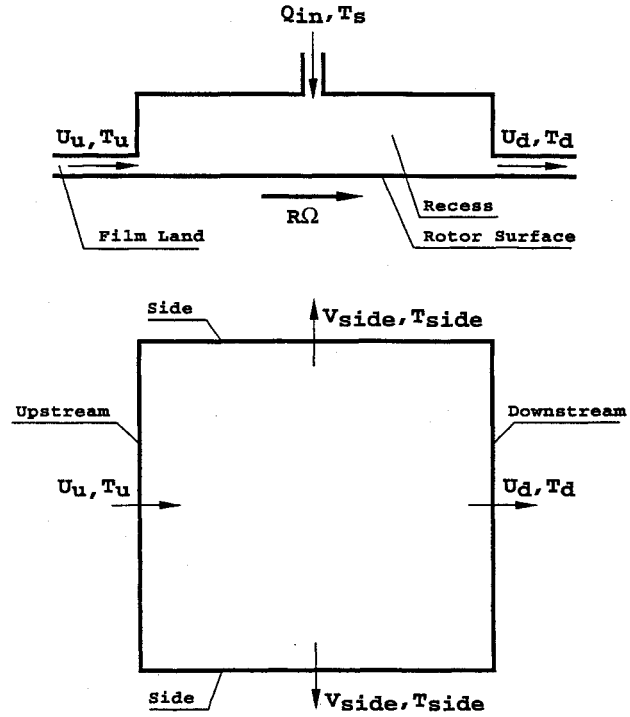

Fig. 4 Conceptual description of global energy balance at a recess.

recess, respectively. The temperatures at the downstream and side edges of the recess are approximately equal to the recess temperature:

$$T_d = T_{\text{side}} = T_r = \text{const} \tag{14}$$

while the temperature at the upstream of the recess is given by

$$T_u = \begin{cases} T_r, & \text{if} \quad (\boldsymbol{U} \cdot \boldsymbol{n}) > 0 \\ \text{upstream values}, & \text{otherwise} \end{cases} \tag{15}$$

III. Boundary Conditions

The boundary conditions for the flow variables are expressed as follows:

1) The pressure, velocity, and temperature fields are continuous and single-valued in the circumferential direction for annular seals and hydrostatic bearings without axial grooves.

2) At the bearing exit plane, the fluid pressure takes a value equal to the discharge or ambient pressure P_a for subsonic operating conditions. The exit pressure may vary circumferentially to represent existing conditions in some turbopump applications.

3) For annular pressure seals, an entrance pressure drop occurs at the seal inlet plane ($y = 0$) and is modeled with a simple Bernoulli equation[10]:

$$P(x, 0) = P_s - \tfrac{1}{2}(1 + \xi_y)\rho V_{(x,0)}^2 \quad \text{if} \quad V_{(x,0)} > 0 \tag{16}$$

with the inlet circumferential velocity prescribed by a swirl ratio α as

$$U(x, 0) = \alpha R\Omega \tag{17}$$

4) At the fluid/journal and the fluid/bearing interfaces, the heat flux to the bounding surfaces Q_s is assumed to be zero. That is, the current thermal model considers the bearing and journal surfaces to be insulated. This condition is representative of turbulent flow, externally pressurized bearings.[10,11]

San Andres[3] provides further details and a thorough discussion on boundary conditions for pad journal bearings and grooved hydrostatic bearings, including the generation of a "ram" pressure at the leading edge of a hydrodynamic pad.

IV. Perturbation and Numerical Analyses

For small-amplitude journal motions about an equilibrium position, all the dependent flow variables as well as the fluid properties are expressed as the superposition of zeroth- and first-order fields representing the steady-state and dynamic motion conditions, respectively. Expansion of the governing equations in the perturbation variables yields zeroth- and first-order flow equations as presented in detail by San Andres.[3] Fluid film forces and rotordynamic coefficients are found by integration of the pressure fields on the journal surface, i.e.,

$$\begin{bmatrix} F_X \\ F_Y \end{bmatrix} = R \sum_{k=1}^{N_{pad}} \int_0^L \int_0^{\theta_{pad}} P_0^k \begin{bmatrix} \cos\theta \\ \sin\theta \end{bmatrix} d\theta\, dy \qquad (18)$$

where P_0^k corresponds to the zeroth-order pressure field for the kth bearing pad. The force coefficients due to journal center displacements are determined from

$$K_{ij} - \omega^2 M_{ij} + i\omega C_{ij} = -R \sum_{k=1}^{N_{pad}} \int_0^L \int_0^{\theta_{pad}} P_j^k h_i \, d\theta\, dy$$

$$\text{with} \quad i, j = X, Y \quad h_X = \cos\theta, \quad h_Y = \sin\theta \qquad (19)$$

and P_X^k, P_Y^k are the dynamic pressure fields for journal motions in the X and Y directions, respectively.[3]

A cell finite difference scheme is implemented to solve the nonlinear differential equations on the film lands,[14] whereas the Newton–Raphson scheme is used to update the recess pressure and to satisfy the mass continuity constraint at each bearing recess.[3] The numerical procedure is based on the forward-marching scheme of Launder and Leschziner[14] and uses the SIMPLEC algorithm introduced by Van Doormaal and Raithby.[24] The SIMPLEC scheme is well known in literature, and details on its superior convergence rate, grid refinement sensitivity, and accuracy have been well documented.[24–26]

Past simpler models from the same author[1,2] have evolved to the present advanced THD model[3,10,11] and responded to the need for more accurate yet efficient computational programs. These codes have been validated with extensive correlations to experimental measurements.[1,2,4,6,7,9] Further validations to experimental force coefficient data for LH_2 HJBs,[27] and water HJBs[5] are reported by Yang et al.[11,28] San Andres[3] also presents detailed comparisons to test force coefficients for an oil-lubricated HJB from Adams et al.,[29] journal bearing load measurements from Tonnesen and Hansen,[30] and numerical predictions by Braun et al.[31] for the performance of LO_2 journal bearings.

In general, calculations show that a relatively small number of grid points for discretization of the bearing surface is typically required to get grid independent results. Less than 2% difference in bearing static and dynamic performance characteristics are obtained when comparing the results from a 67 × 16 grid (number of circumferential points × axial points) with those from a 85 × 26 grid for the bearing cases reported in this article. Note also that the applicability of the analysis and computer program developed[3] include fluid film bearings for industrial applications in the laminar-flow regime with conventional lubricants.

Several empirical parameters are used in the analysis of hydrostatic bearings and annular pressure seals. Entrance loss coefficients ξ_y, ξ_x and rotor (journal) and stator (bearing) surface roughnesses r_j, r_B are needed for seals and HJBs, while orifice discharge coefficients C_d are also required for hydrostatic bearings. Lindsey[6] presents a sensitivity analysis for annular seals, and Kurtin et al.,[4] Mosher,[7] and Franchek et al.[12] present similar studies for hydrostatic bearings. These references describe detailed comparisons between numerical predictions based on the present model and experimental measurements performed on water-lubricated seals and hydrostatic bearings at an existing test facility.[5] The sensitivity analysis involved changing an input parameter by ± 10% from its estimated experimental value for each operating condition while the other input parameters were kept invariant. The maximum difference between the numerical prediction and experimental value for each case was then compared with the maximum difference from the original results. Then, a relative sensitivity was determined by dividing the percentage change in maximum difference of the calculated parameter by the percentage change in the input parameter (10%).[12] The studies found that flow rate and direct stiffness coefficients are particularly sensitive to changes in C_d for HJBs and less sensitive to variations in the entrance loss coefficients. On the other hand, flow rate and direct stiffness coefficients for annular pressure seals are highly sensitive to the changes in inlet loss coefficient ξ_y and surface roughness conditions. Other force coefficients and the whirl frequency ratio for HJBs are particularly insensitive to variations in the empirical parameters (C_d and $\xi_{x,y}$). For further details on the sensitivity analyses and major results, the interested reader is encouraged to seek the references cited.

V. Results and Discussion

A one-to-one comparison for bearing performance in terms of flow, load capacity, and rotordynamic force coefficients for a hydrostatic bearing and a damping bearing (parallel-land damper seal) operating in LO_2 is presented here. The HJB and the damping bearing are designed to replace the pump-end duplex ball bearings in the LO_2 HPOTP. The fluid operating conditions (pressure and temperature) as well as the actual bearing clearance, and most importantly, the load supported by the bearings, are a function of the rotating speed of the pump. Information relevant to the load characteristics in the HPOTP were obtained from Shoup[32] and the fluid operating conditions directly extracted from Heshmat.[33] The hydrostatic bearing has six recesses of rectangular shape and orifice restrictors, while the damping bearing consists of two parallel annular seals of convergent tapered clearance separated by a deep feeding central groove.[34] The seals have a rough stator surface of knurled type while the hydrostatic bearing and journal surfaces are perfectly smooth. The damping bearing is also sometimes referred to as an annular hydrostatic bearing.[35] Figure 5 shows a description of the bearing geometries along with the values of actual clearances, supply, and discharge pressures and supply temperature for LO_2, and the nominal load acting on the bearings as the operating speed increases from 14,035 to 30,367 rpm. Note that the load and pressures are proportional to the second power of the rotational speed. At the nominal operating conditions, here taken as 26,000 rpm, the operating clearance in the HJB is equal to 0.175 mm, while the inlet and exit clearances in the damping bearing are equal to 0.221 and 0.129 mm (ratio = 1.715), with an average clearance identical to that of the hydrostatic journal bearing.

The hydrostatic bearing is designed for operation at the nominal speed with a concentric pressure ratio equal to 0.60 to provide maximum direct stiffness coefficients. On the other hand, the ratio of inlet to discharge clearance in the damping bearing has been optimized to also obtain the largest direct stiffness coefficients. The maximum specific load (load divided by bearing projected area) is equal to 6.55 MPa (950 psi) and 7.22 MPa (1048 psi) for the hydrostatic bearing and damper seal, respectively. These specific loads are large considering the nature of the bearing application with a fluid of very low viscosity such as LO_2. The calculations for the static and dynamic performance characteristics of the HJB and

Hydrostatic Bearing: Number of recesses **Nrec** = 6

Diameter (D)	Length (L)	Clearance (C*)	Recess Depth	Recess Axial Length(l)	Recess Circ. length(b)
85.1 mm	48.85 mm	175.2μm	508μm	24.42 mm	22.3 mm
(3.35 in)	(1.92 in)	(6.9 mils)	(20 mils)	(0.96 in)	(0.88 in)

journal and bearing surface conditions: **smooth.**
L/D=0.57; **Hr/C**=2.9, **l/L**=0.5, Recess area ratio=0.25, **C/R** =0.0041
Orifice C_d=0.90; diameter **do** = 4.44 mm
Recess edge coefficients ξ_{xu}=0.0; ξ_{xd}=0.50; ξ_y=0.0

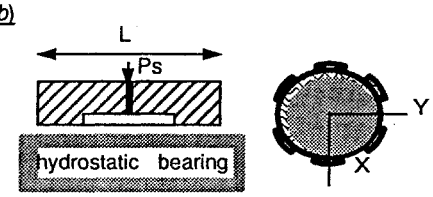

Damping Bearing: Two parallel seal lands (2 x L) (groove width unspecified)

Diameter (D)	Length (L)	Inlet Clearance	Exit Clearance	Ratio	Average Clearance
85.1 mm	22.2 mm	221.3μm	129.1μm	1.71	175.2μm
(3.35 in)	(0.874 in)	(8.7 mils)	(5.08 mils)		(6.9 mils)

journal surface smooth, bearing surface rough, r_B/C = 0.044 (Knurled)
Seal entrance coefficient ξ_y=0.25
Inlet swirl ratio α= 0.50

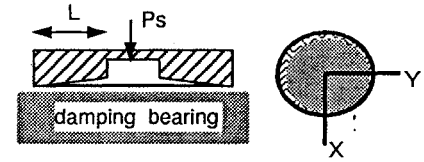

Operating Conditions for both bearings:

Speed cpm	Psupply MPa	Pa	Tsupply K	Tsat K	Load N	Reynolds# Rec	Average Clearance* (μm)
14,035	16.00	1.654	102.77	128.9	5,828	72,816	180
19,732	29.59	1.792	107.22	130.5	11,519	100,700	177.7
26,000	39.60	2.089	110.55	133.7	20,000	130,130	175.2
28,340	43.60	2.434	111.33	137.0	23,762	143,720	174.3
30,367	55.69	2.551	115.00	138.0	27,282	147,600	173.2

Fluid Properties: **LO_2 (liquid oxygen)** at 110.6 K (200R)

P (MPa)	ρ (kg/m3)	μ (E-3 Pa.s)	Cp(J/kg-K)
39.60	1134.4	0.177	1,606.4
2.09	1038.1	0.124	1,827.2

Fig. 5 Geometry and operating conditions of a hydrostatic bearing and a damping bearing for load support in the LOx SSME-HPOTP.

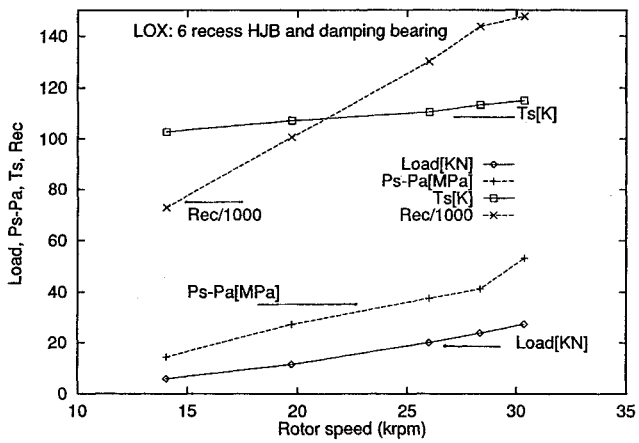

Fig. 6 Supply temperature, pressure drop, circumferential Reynolds number and load vs rotational speed for LO_x six-recess hydrostatic bearing and damping bearing.

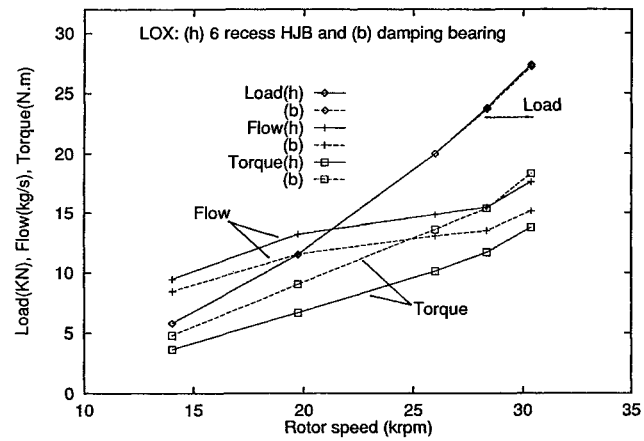

Fig. 7 Flow rate, applied load, and drag torque vs rotational speed for LO_x (h) six-recess HJB and (b) damping bearing.

damping bearing are performed using an adiabatic journal (rotor) and bearing (stator) thermal model.

Numerical calculations for the damping bearing are performed only for the thin land (seal) portion and then multiplied by two. The central groove and its effect on load capacity and dynamic force coefficients are altogether neglected. This oversimplification seems appropriate as a first attempt to correlate the performance of the HJB and the damping bearing. However, it is now known that central feeding grooves do have a pronounced effect on the dynamic force response of fluid film bearings, in particular with regard to inertia and cross-coupled damping force coefficients.[6,36]

Figure 6 depicts the fluid supply temperature, pressure drop, and expected load to be carried by the HJB or the damping bearing as the rotational speed of the pump increases. The largest load of 27,282 N (6137 lb) corresponds to the highest operating speed. The figure also shows the values of the nominal circumferential flow Reynolds number $Re_c = \rho_* R\Omega c_*/\mu_*$ to range from approximately 70,000 to 150,000 as the rotor speed rises. Figure 7 shows the HJB and damping bearing flow rates and drag torques as the journal speed increases.

The hydrostatic bearing (h) shows approximately 14% more flow rate than the damping bearing (b), while the HJB produces approximately 27% less drag torque than the seals at the largest operating speed. These results are a direct consequence of the rough stator surface in the damping bearing.

Figure 8 presents the journal operating eccentricity and attitude angle as well as the maximum temperature rise in the HJB and damping bearing as the operating speed increases. Note that as the speed rises so does the applied load at a rate proportional to the journal speed squared. The load for the HJB is directed towards the bottom of a bearing recess (X direction). The dimensionless journal eccentricity is given here as the ratio between the journal off-center displacement divided by the nominal clearance at 26,000 rpm, i.e., 0.175 mm. Note that the attitude angle is less than 10 deg for both bearings, and the journal eccentric displacement is rather moderate considering the magnitude of the loads applied. The low value in the attitude angle indicates dominance of hydrostatic effects over hydrodynamic effects. The maximum temperature in the film lands of the hydrostatic and damping bearings increases rapidly with journal speed. The HJB shows a larger thermal differential between the bearing supply condition and discharge planes. The results also indicate that both bearings operate well below the critical temperature of T_c = 154.6 K (278°R) for LO_2.

Figures 9–11 present the synchronous stiffness, damping, and inertia force coefficients vs the rotational speed for the HJB and damping bearings, respectively. The similar values

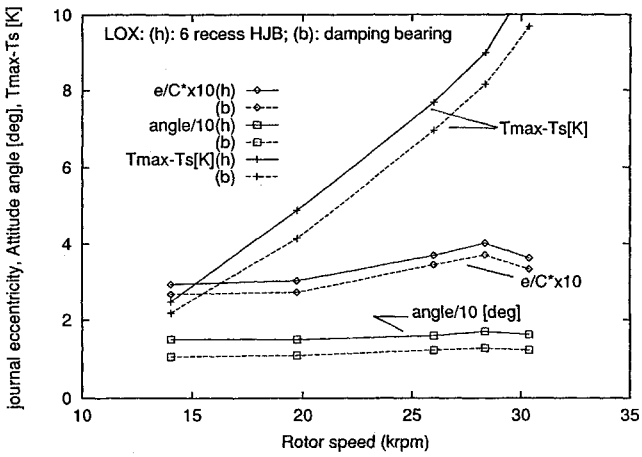

Fig. 8 Journal eccentricity, attitude angle, and maximum temperature rise vs rotational speed for LO_x (h) six-recess HJB and (b) damping bearing.

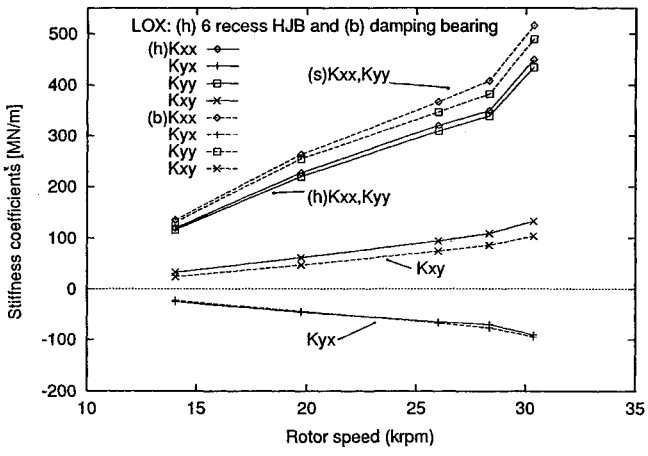

Fig. 9 Synchronous stiffness coefficients K_{ij} vs rotational speed for LO_x (h) six-recess HJB and (b) damping bearing.

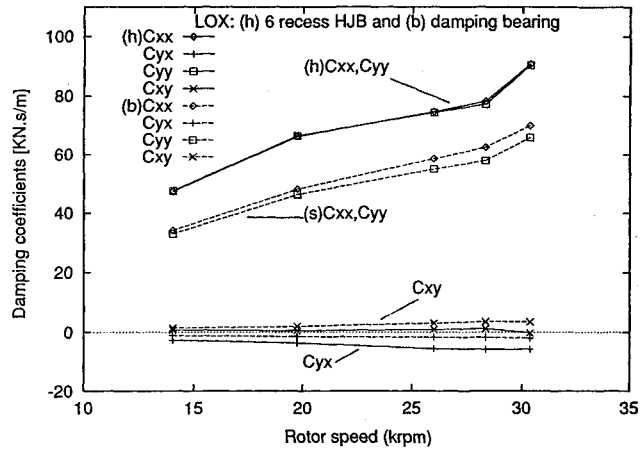

Fig. 10 Synchronous damping coefficients C_{ij} vs rotational speed for LO_x (h) six-recess HJB and (b) damping bearing.

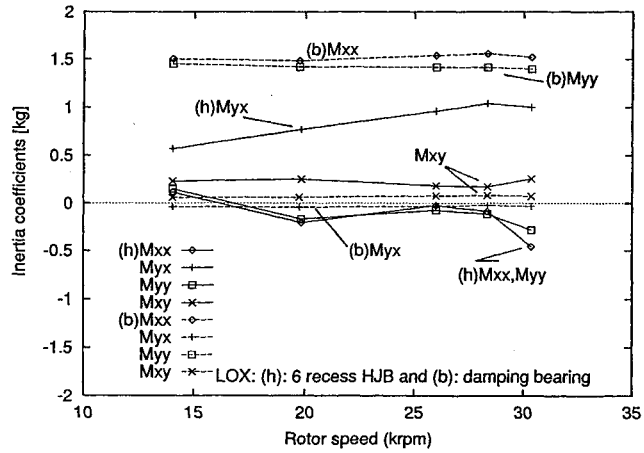

Fig. 11 Inertia force coefficients M_{ij} vs rotational speed for LO_x (h) six-recess HJB and (b) damping bearing.

between the direct coefficients (e.g., K_{XX} and K_{YY}) and cross-coupled coefficients (e.g., K_{XY} and $-K_{YX}$) denote that the HJB and damper bearing seal have very uniform force coefficients as the operating eccentricity (and load) increases with the operating speed. Figure 9 shows an HJB with slightly smaller direct stiffness coefficients (K_{XX} and K_{YY}) than the damping bearing, while its cross-coupled stiffness (K_{XY}) is larger. Note the dominance of hydrostatic (direct) coefficients over the cross-coupled coefficients induced solely by journal rotation.

Figure 10 shows the hydrostatic bearing to have larger direct damping coefficients (C_{XX} and C_{YY}) than the damping bearing (approximately 47% higher). These results produce at the largest journal speed a whirl frequency ratio (WFR) equal to 0.39 and 0.45 for the HJB and damping bearing, respectively. Thus, in this example when the inlet swirl ratio is equal to 0.50, the HJB offers slightly better dynamic stability characteristics than the damping bearing. The values of WFR quoted remain approximately constant for all speeds studied. Note that low-frequency pneumatic-hammer effects are of little importance here since LO_2 is nearly incompressible at the operating conditions and the bearing recesses are quite shallow (H_r/C = 2.9).

Figure 11 shows the damping-bearing direct inertia force coefficients (M_{XX} and M_{YY}) to be on the order of 1.5 kg and larger than the HJB direct inertia coefficients. The reason for this lies on the tapered geometry of the damper bearing seal with a small clearance at the exit plane. The cross-coupled inertia coefficients (M_{XY} and M_{YX}) are small in nature. Here,

it is noted that in practice the direct inertia coefficients for the damping bearing will be much larger than the ones predicted. The central feeding groove acts as a parallel inertia and compliance to the seal lands, increases the magnitude of the inertia coefficients, and may reduce substantially the direct dynamic stiffness of the damping bearing.[35] Experimental results showing this behavior have been reported recently by Lindsey.[6]

It is worth noting that the original study included a three-pad journal bearing with a clearance similar to that of the HJB, but with a bearing preload of 0.076 mm. The results are not reproduced here because the hydrodynamic bearing produced a rather large temperature rise, and offered a low load capacity in comparison to those obtained from the six-recess hydrostatic and damping journal bearings.[3]

VI. Conclusions

Accurate prediction of the performance and static and dynamic force characteristics of process-liquid, turbulent-flow fluid film bearings requires a thermohydrodynamic analysis. A set of bulk-flow equations for mass conservation, momentum, and energy transport describes the fluid motion in turbulent flow bearings with cryogenic liquids. The nonlinear flow equations are solved with a finite difference scheme combined with the Newton–Raphson method to satisfy the mass continuity requirement at each hydrostatic bearing recess. Published comparisons between numerical results and experimental data of turbulent flow water HJBs and seals are favorable and demonstrate the validity of the THD analysis and the computer program developed.

Numerical predictions show that properly designed hydrostatic bearings and damping journal bearings can support effectively the loads expected in the LO_2 HPOTP. The results indicate that an HJB or a damping bearing will operate at low journal eccentricities with uniform force coefficients. The case studied shows an important application of the fluid hydrostatic principle where sound engineering practice utilizes the available pressure differential in a cryogenic turbopump to provide a reliable fluid film bearing support.

Acknowledgments

This research was funded under NASA Grant NAG3-1434. Acknowledgments are due to NASA Lewis Research Center for its support, and in particular to James Walker for his interest on this work.

References

[1]San Andres, L., "Analysis of Variable Fluid Properties, Turbulent Annular Seals," *Journal of Tribology*, Vol. 113, No. 4, 1991, pp. 694–702.

[2]San Andres, L., "Analysis of Turbulent Hydrostatic Bearings with a Barotropic Cryogenic Fluid," *Journal of Tribology*, Vol. 114, No. 4, 1992, pp. 755–765.

[3]San Andres, L., "Thermohydrodynamic Analysis of Cryogenic Liquid Turbulent Flow Fluid Film Bearings," Texas A&M Univ., Research Progress Rept., NASA Grant NAG3-1434, College Station, TX, Dec. 1993.

[4]Kurtin, K. A., Childs, D., San Andres, L., and Hale, K., "Experimental Versus Theoretical Characteristics of a High Speed Hybrid (Combination Hydrostatic and Hydrodynamic) Bearing," *Journal of Tribology*, Vol. 115, No. 1, 1993, pp. 160–168.

[5]Childs, D., and Hale, K., "A Test Apparatus and Facility to Identify the Rotordynamic Coefficients of High-Speed Hydrostatic Bearings," *Journal of Tribology*, Vol. 116, 1994, pp. 337–344.

[6]Lindsey, T., "Experimental vs. Theoretical Comparison of the Effects of Taper on the Rotordynamic Coefficients in Short Smooth Annular Seals Used in High-Speed Turbomachinery," M.S. Thesis, Texas A&M Univ., College Station, TX, May 1993.

[7]Mosher, P., "Effect of Design Parameter Variations on Hybrid (Combination Hydrostatic and Hydrodynamic) Bearings for Use in High Speed Turbomachinery," M.S. Thesis, Texas A&M Univ., College Station, TX, May 1993.

[8]Franchek, N., and Childs, D., "Experimental Test Results for Four High-Speed, High-Pressure Orifice Compensated Hybrid Bearings," *Journal of Tribology*, Vol. 116, No. 1, 1994, pp. 147–153.

[9]Franchek, N., Childs, D., and San Andres, L., "Theoretical and Experimental Comparisons for Rotordynamic Coefficients on a High-Speed, High-Pressure, Orifice Compensated Hybrid Bearing," American Society of Mechanical Engineers Paper 94-Trib-3, 1994.

[10]Yang, Z., San Andres, L., and Childs, D., "Thermal Effects in Cryogenic Liquid Annular Seals, Part I: Theory and Approximate Solution; Part II: Numerical Solution and Results," *Journal of Tribology*, Vol. 115, No. 2, 1993, pp. 285–290.

[11]Yang, Z., San Andres, L., and Childs, D., "Thermohydrodynamic Analysis of Process Liquid Hydrostatic Bearings in Turbulent Regime, I: Theory, II: Numerical Solution and Results," *Journal of Applied Mechanics* (to be published).

[12]Di Pasquantonio, F., and Sala, P., "Influence of Thermal Field on the Resistance Law in Turbulent Bearing-Lubrication Theory," *Journal of Tribology*, Vol. 106, No. 3, 1984, pp. 368–376.

[13]Hirs, G. G., "A Bulk-Flow Theory for Turbulence in Lubricant Films," *Journal of Lubrication Technology*, Vol. 95, No. 1, 1973, pp. 137–146.

[14]Launder, B. E., and Leschziner, M., "Flow in Finite Width Thrust Bearings Including Inertial Effects, I—Laminar Flow, II—Turbulent Flow," *Journal of Lubrication Technology*, Vol. 100, 1978, pp. 330–345.

[15]Childs, D., *Turbomachinery Rotordynamics*, Wiley, New York, 1993, pp. 233–235.

[16]San Andres, L., and Velthuis, J. F. M., "Laminar Flow in a Recess of a Hydrostatic Bearing," *Tribology Transactions*, Vol. 35, No. 4, 1992, pp. 736–744.

[17]Braun, M. J., Don, Q., and Choy, F. K., "The Effects of a Hydrostatic Pocket Aspect Ratio, and Its Supply Orifice Position and Attack Angle on Steady-State Flow Patterns, Pressure and Shear Characteristics," *Journal of Tribology*, Vol. 115, No. 4, 1993, pp. 678–685.

[18]Braun, M. J., Zhou, Y., and Choy, F. K., "Transient Flow Patterns and Pressure Characteristics in a Hydrostatic Pocket," *Journal of Tribology*, Vol. 116, No. 1, 1994, pp. 139–146.

[19]Ho, Y. S., and Chen, N. N., "Pressure Distribution in a Six-Pocket Hydrostatic Journal Bearing," *Wear*, 1984, Vol. 98, pp. 89–100.

[20]Chaomleffel, J. P., and Nicholas, D., "Experimental Investigation of Hybrid Journal Bearings," *Tribology International*, Vol. 19, No. 5, 1986, pp. 253–259.

[21]Reddecliff, J. M., and Vohr, J. H., "Hydrostatic Bearings for Cryogenic Rocket Engine Turbopumps," *Journal of Lubrication Technology*, Vol. 91, 1969, pp. 557–575.

[22]Constantinescu, V. N., and Galetuse, S., "Pressure Drop due to Inertia Force in Step Bearings," American Society of Mechanical Engineers Paper 75-Lub-34, 1975.

[23]Artiles, A., Walowit, J., and Shapiro, W., "Analysis of Hybrid Fluid Film Journal Bearings with Turbulence and Inertia Effects," *Advances in Computer Aided Bearing Design*, American Society of Mechanical Engineers Publication G0020, 1982, pp. 25–52.

[24]Van Doormaal, J. P., and Raithby, G. D., "Enhancements of the SIMPLE Method for Predicting Incompressible Fluid Flows," *Numerical Heat Transfer*, Vol. 7, 1984, pp. 147–163.

[25]Van Doormaal, J. P., and Raithby, G. D., "An Evaluation of the Segregated Approach for Predicting Incompressible Fluid Flow," American Society of Mechanical Engineers Paper 85-HT-9, 1985.

[26]Jang, D. S., Jetli, R., and Acharya, S., "Comparison of the PISO, SIMPLER, and SIMPLEC Algorithms for the Treatment of the Pressure-Velocity Coupling in Steady Flow Problems," *Numerical Heat Transfer*, Vol. 10, No. 2, 1986, pp. 209–228.

[27]Butner, M., and Murphy, B., "SSME Long Life Bearings," NASA CR-179455, 1986.

[28]Yang, Z., San Andres, L., and Childs, D., "Process Liquid Turbulent Flow Hydrostatic Bearings: Analysis and Tests for Rotordynamic Coefficients," *Proceedings of the IFToMM Rotordynamics Conference* (Chicago), 1994, pp. 233–241.

[29]Adams, M., Sawicki, J. T., and Capaldi, R., "Experimental Determination of Hydrostatic Journal Bearing Coefficients," International Conf. in Vibrations in Rotating Machinery, Vibration Inst., Paper C432/145, IMechE 1992-6, Willowbrook, IL, Sept. 1992.

[30]Tonnesen, J., and Hansen, P. K., "Some Experiments on the Steady State Characteristics of a Cylindrical Fluid-Film Bearing Considering Thermal Effects," *Journal of Lubrication Technology*, Vol. 103, 1981, pp. 107–114.

[31]Braun, M. J., Wheeler, R. L., III, and Hendricks, R. C., "Ther-

mal Shaft Effects on Load-Carrying Capacity of a Fully Coupled, Variable Properties Cryogenic Journal Bearing," *STLE Tribology Transactions*, Vol. 30, No. 2, 1987, pp. 282–292.

[32]Shoup, T., private communication, Sverdrup–NASA Marshall Space Center, Huntsville, AL, Oct. 1993.

[33]Heshmat, H., "Investigation of Foil Bearings for Use in High-Thrust Liquid Rocket Engines," NASA CR-197099, April 1991.

[34]Von Pragenau, G. L., "Damping Bearings for Turbomachinery," NASA TP 3092, Vol. II, 1990, pp. 155–162.

[35]Scharrer, J. K., Hibbs, R. I., and Nolan, S., "Extending the Life of the SSME HPOTP Through the Use of Annular Hydrostatic Bearings," AIAA Paper 92-3401, July 1992.

[36]Arauz, G., and San Andres, L., "Effect of a Circumferential Feeding Groove on the Force Response of a Short Squeeze Film Damper," *Journal of Tribology*, Vol. 116, No. 2, 1994, pp. 369–377.